

## Uncertainty in wave energy resource assessment. Part 1: Historic data

Edward B.L. Mackay<sup>a,\*</sup>, AbuBakr S. Bahaj<sup>a</sup>, Peter G. Challenor<sup>b</sup>

<sup>a</sup>Sustainable Energy Research Group, School of Civil Engineering and the Environment, University of Southampton, Highfield, Southampton SO17 1BJ, UK

<sup>b</sup>Ocean Observing and Climate Group, National Oceanography Centre, Southampton SO14 3ZH, UK

### ARTICLE INFO

#### Article history:

Received 16 September 2009

Accepted 16 October 2009

Available online 12 November 2009

#### Keywords:

Wave energy resource  
Numerical wave model  
Hindcast  
Calibration  
Uncertainty

### ABSTRACT

The uncertainty in estimates of the energy yield from a wave energy converter (WEC) is considered. The study is presented in two articles. This first article deals with the accuracy of the historic data and the second article considers the uncertainty which arises from variability in the wave climate. Estimates of the historic resource for a specific site are usually calculated from wave model data calibrated against in-situ measurements. Both the calibration of model data and estimation of confidence bounds are made difficult by the complex structure of errors in model data. Errors in parameters from wave models exhibit non-linear dependence on multiple factors, seasonal and interannual changes in bias and short-term temporal correlation. An example is given using two hindcasts for the European Marine Energy Centre in Orkney. Before calibration, estimates of the long-term mean WEC power from the two hindcasts differ by around 20%. The difference is reduced to 5% after calibration. The short-term temporal evolution of errors in WEC power is represented using ARMA models. It is shown that this is sufficient to model the long-term uncertainty in estimated WEC yield from one hindcast. However, seasonal and interannual changes in model biases in the other hindcast cause the uncertainty in estimated long-term WEC yield to exceed that predicted by the ARMA model.

© 2009 Elsevier Ltd. All rights reserved.

### 1. Introduction

Before a wave farm is installed developers and planners need to have an estimate of the energy that will be produced over the expected life time. Like other sources of renewable energy, ocean waves are a variable resource, impossible to predict precisely. This increases the risk associated with the development of a wave energy farm, since the upfront cost of a project is large and the return is variable and imprecisely known. It is therefore necessary to estimate the expected yield from the wave farm, the variability in power production and confidence bounds on these estimates.

The uncertainty in estimates of the electrical power which will be produced by a wave farm can be split into three categories:

- 1 Uncertainty in future wave conditions.
- 2 Uncertainty in conversion from wave energy to electrical energy.
- 3 Uncertainty in availability of machines.

This paper will focus on the uncertainty in future wave conditions but it is worth making some notes on the other sources of

uncertainty as well. The electrical energy produced by a wave energy converter (WEC) in a given sea state is dependent on the full directional wave spectrum. However, for the purposes of estimating the yield it is useful to describe the response in terms of a small number of parameters. Most device manufacturers specify the power produced by a WEC in a 'power matrix' in terms of the significant wave height,  $H_s$ , and energy period,  $T_e$ . The power matrices are usually calculated from numerical simulation of the WEC using theoretical spectral shapes such as Pierson-Moskowitz (PM) or JONSWAP (see e.g. [1]), and are validated using a combination of scale-model tank tests and sea trials with prototype devices. For real wave spectra there will be some deviation in the spectral shape and directional distribution from theoretical forms, which will result in differences in the power produced from the values specified in the power matrix.

Parameterising the WEC response solely in terms of  $H_s$  and  $T_e$  leads to uncertainties in estimates of power for a given sea state, but at this stage of the industry, where few experimental or hard data exist, it is a necessary approximation. On the whole, the effect of parameterisation is less important for higher  $H_s$ , since spectra tend toward standard shapes in larger seas. Kerbiriou et al. [2] have shown that partitioning directional spectra into separate sea states improves accuracy compared to using a simple parametric representation of the whole spectrum when estimating the performance

\* Corresponding author. Fax: +44(0) 7861 383995

E-mail address: [e.mackay@soton.ac.uk](mailto:e.mackay@soton.ac.uk) (E.B.L. Mackay).

of the SEAREV device. Once further data has been gathered on the effects of varying spectral shapes and directional distributions, this can be factored into the estimated energy yield in a probabilistic manner. This is discussed further in Section 6.

Interactions between WECs within arrays will cause differences in the power absorbed compared to an isolated device. This introduces a further level of uncertainty into the conversion from wave energy to electrical energy. There has been a considerable amount of work on the theoretical aspects of WEC interaction effects (see [3] for a brief overview). Millar et al. [4] take a slightly different approach in order to examine the impact of an offshore wave farm on the shoreline wave climate, but their method could be applied to model array losses. They use the spectral wave model SWAN [5] to examine the effect of a generic WEC removing energy at various points in the wave field. This paper will focus on modelling the uncertainty in the predicted yield of a single device. Array losses can be factored into calculations when more precise information is available.

The third category of uncertainty mentioned above is perhaps the most difficult to quantify. Mechanical failures are inherently unpredictable in a new technology. As operational experience is gained maintenance requirements will be better understood and it will be possible to estimate the availability of machines. At present it is difficult to put a realistic figure on this type of uncertainty.

The aim of this paper is to estimate the uncertainty in predicted energy yield resulting from uncertainty in future wave conditions. Estimates of future wave conditions are based on historic conditions. The accuracy is limited by the accuracy of the historic data and the variability in the resource. Due to the length and complexity of the analysis, the work will be presented in two articles. This first article deals with uncertainty in the historic data and the second article [6] deals with uncertainty in the future wave conditions resulting from variability in the resource.

## 2. Summary of approach

In order to get a reasonable estimate of the long-term mean and interannual variability in the power produced by a WEC at a specific site a long record of wave conditions is required. It is rare that at a site of a proposed wave farm there will be an existing long-term dataset. In absence of a long record for the site of interest, an approach similar to the Measure-Correlate-Predict (MCP) method used by the wind energy industry can be applied. In the MCP procedure short-term measurements recorded at the site of a proposed development (the predictor site) are correlated with concurrent measurements taken at a nearby reference site for

which long-term data exists. This calibration is then applied to the historic data at the reference site to estimate the historic climate at the predictor site.

The US and Canada have an extensive network of offshore wave buoys which can be used as long-term reference datasets. Recent assessments of wave energy potential from these buoys are given in [7, 8]. In Europe there are fewer offshore buoys. Halliday and Douglas [9] have presented a survey of the long-term wave data available in UK waters. They note that there is relatively little in-situ data available for the most energetic locations and that it would aid wave energy development if coverage was increased in these areas.

Where there are no long-term measurements to use as reference datasets, some authors have proposed the use of data from numerical wave models as a long-term reference [10–12]. Mollison [10] proposed that offshore data from ocean-scale models could be used as the boundary conditions of a smaller scale shallow-water wave model, which is used to estimate the wave conditions at the site of interest. Since wave model data are estimates rather than measurements, Mollison [10] suggests that the model data should be calibrated against nearby buoy measurements before use. Barstow et al. [11] take a similar approach, but use satellite altimeter measurements to calibrate the offshore wave model data, before using it to drive a nearshore model. This approach is now common in wave energy resource studies. Pitt [12] compared estimates of wave power from the UK Met Office wave model to estimates from buoy measurements at the location of the proposed Wave Hub site in South West Britain. Several recent studies [13–15] have used data from the nearshore model SWAN [5] with boundary conditions from the WAM model [16] to estimate the nearshore wave resource.

However, the issue of uncertainty in energy yield predictions, necessary for the economic assessment of a wave energy project, has not yet been addressed. This is in part because until recently the industry has not required such detailed calculations. With the first full scale devices being deployed at present and rapid expansion of the wave energy industry foreseen over the next decade, the problem of making accurate yield predictions with quantified uncertainty needs to be considered. As mentioned earlier, the uncertainty in the historic data is discussed in this first article and the second article [6] considers uncertainty arising from the variability of the resource.

The uncertainty in the estimate of the historic WEC yield is examined using two hindcasts for the European Marine Energy Centre (EMEC) in Orkney. The Pelamis wave energy converter is used as an example. The power matrix for an early version of the Pelamis WEC is given in Table 1. It will be shown later on that over

**Table 1**  
Power matrix for an early version of the Pelamis WEC, values in kW.

		$T_e$ [s]																
		5.0	5.5	6.0	6.5	7.0	7.5	8.0	8.5	9.0	9.5	10.0	10.5	11.0	11.5	12.0	12.5	13.0
$H_s$ [m]	0.5	Idle	Idle	Idle	Idle	Idle	Idle	Idle	Idle	Idle	Idle	Idle	Idle	Idle	Idle	Idle	Idle	Idle
	1.0	Idle	22	29	34	37	38	38	37	35	32	29	26	23	21	Idle	Idle	Idle
	1.5	32	50	65	76	83	86	86	83	78	72	65	59	53	47	42	37	33
	2.0	57	88	115	136	148	153	152	147	138	127	116	104	93	83	74	66	59
	2.5	89	138	180	212	231	238	238	230	216	199	181	163	146	130	116	103	92
	3.0	129	198	260	305	332	340	332	315	292	266	240	219	210	188	167	149	132
	3.5		270	354	415	438	440	424	404	377	362	326	292	260	230	215	202	180
	4.0			462	502	540	546	530	499	475	429	384	366	339	301	267	237	213
	4.5			554	635	642	648	628	590	562	528	473	432	382	356	338	300	266
	5.0				739	726	731	707	687	670	607	557	521	472	417	369	348	328
	5.5				750	750	750	750	750	737	667	658	586	520	496	446	395	355
	6.0					750	750	750	750	750	750	711	633	619	558	512	470	415
	6.5					750	750	750	750	750	750	750	743	658	621	579	512	481
	7.0						750	750	750	750	750	750	750	750	676	613	584	525
	7.5							750	750	750	750	750	750	750	750	686	622	593
	8.0								750	750	750	750	750	750	750	750	690	625

an 8-year period covered by both datasets, the mean power produced by the Pelamis calculated from each hindcast differs by over 20%. It is clear that one or both models produce significantly biased estimates. In this article the calibration of wave model data is discussed and a method is proposed to calculate confidence bounds for estimates of WEC yield from calibrated model data. The paper begins with a description of the errors in model data in Section 3. In Section 4 techniques for estimating model errors are discussed. In Section 5 these techniques are applied to calibrate the hindcasts for the EMEC site. In Section 6 the estimation of confidence bounds on the estimate of energy yield from the calibrated hindcasts is discussed, and in Section 7 the two calibrated hindcasts are compared in more detail. In Section 8 the results are discussed and conclusions are presented.

### 3. Errors in wave model data

Understanding the features of errors in model data is vital both for calibration purposes and for the calculation of the uncertainty of derived wave energy statistics. Error sources can be viewed as either internal or external to the model. The internal sources of error are the formulation of model physics or 'sources terms' and the numerical resolution, while external errors refer to errors in the input data, primarily the wind field. An in depth review of the present state of the art and limiting factors in wave modelling is given in [17]. In this section we are concerned with a description rather than diagnosis of model errors.

Modelled wave spectra can be considered an estimate of the average conditions over the grid spacing and time step used in the model. Typically, global or oceanic scale wave models will be run with a grid spacing somewhere between  $0.5^\circ$  and  $3^\circ$  (about 50–300 km) with a time step of 3 or 6 h. Measured data are obtained over a smaller scale, with data from buoys representing a point average over time (between 20 min and 1 h) and altimeter data representing an instantaneous spatial average over an area of 5–10 km in diameter. The spatial and temporal variability of wave conditions will therefore result in differences between measurements and modelled data, even if both are perfectly accurate. The larger scales over which wave models estimate conditions result in time series of model data appearing smoother than those from in-situ measurements. It can also lead to small intense pressure systems being subject to some smoothing, resulting in systematic underestimation of peak wind speeds and hence peak wave heights [18].

The calibration of wave model data involves estimating the mean error under a given set of conditions. Modelling the random errors is necessary for estimating confidence bounds. It can be difficult to distinguish between the mean and random model errors, since the error at a given location is the integrated effect of mean (predominantly internal) and random (predominantly external) errors over the whole wave field. Both the mean and random components will have a complex dependence on the actual wave conditions. For instance the bias in a model estimate of  $H_s$  may have a dependence on the actual  $H_s$ , period, spectral shape, swell age, etc. Due to the way that errors occur in wave models and propagate through the model domain, the biases are non-stationary with location and with time. Janssen [19] presents a particularly clear illustration of the non-stationary biases in spectra from the European Centre for Medium Range Weather Forecasts (ECMWF) WAM model. A plot of the bias in spectral energy binned by frequency shows that the model tends to over-predict energy at lower frequencies in the Northern Hemisphere summer and much less in the winter time. Moreover, the magnitude of this bias and its dependence on both frequency and time of year changes from year to year. He notes that the main reasons for

the changing biases are that large swells generated in the Southern Ocean in the Southern Hemisphere winter time are not well modelled due to the formulation of the dissipation source term and unresolved islands and atolls.

This goes to show that it is difficult to define and adjust for a 'mean error component' since varying conditions lead to varying amounts of internal and external errors occurring and aggregating over the model domain. Therefore errors in wind seas and young swells can be expected to have different characteristics to older swells that have propagated further, increasing uncertainties.

A further reason for non-stationary biases in model data is changes made to the models themselves. This is more of an issue for archived data from operational models than for hindcasts. However, despite the fact that hindcasts are run with a constant model setup, the quality of the input wind fields and assimilated wave data may be varying.

As well as biases changing with time and location, the random error will persist in both time and location. For instance models will tend to over or under predict the intensity of an entire storm, which leads to correlation of errors up to a few days.

Additionally errors in various parameters can be correlated. At high sea states, since wave spectra tend toward standard PM or JONSWAP type forms, an overestimate in model  $H_s$  will result in an overestimate of period as well. This correlation of errors between parameters means that one needs to be careful when calibrating model data, since adjusting model parameters independently may lead to changes in the shape of their joint distribution.

Finally, we note that modelled data may be subject to temporal offsets, with the model predicting that a storm arrives slightly early or late. This type of error is sometimes referred to as a 'jitter error'. Jitter errors are not so important when calculating long-term mean statistics from modelled data, but are important for validation purposes where concurrent modelled and measured data are compared.

To summarise, the main features of the errors in model data are:

- The bias and variance of modelled parameters may depend on multiple factors such as  $H_s$ ,  $T_e$ , swell age, etc.
- The bias and variance of the modelled parameters may be non-stationary with both time and location.
- Errors in parameters exhibit short-term auto-correlation.
- There may also be correlation of errors between parameters, e.g. errors in  $H_s$  and  $T_e$  may be correlated.
- There may be temporal offsets or 'jitter errors' in modelled parameters.

## 4. Techniques for estimating model errors

### 4.1. Published studies

Model errors are estimated by comparing collocated modelled and measured parameters, where the measurements are usually from wave buoys or satellite altimeters. Various techniques have been proposed to determine the errors. If there is reason to believe that the model bias may be a linear function of a model parameter then linear regression can be used [20,21]; to test for non-linearities the bias and standard deviation of model data, can be plotted against integrated buoy parameters such as  $H_s$  and  $T_p$  [20] or the bias can be calculated in discrete frequency bands [19,22]. A more sophisticated approach was implemented by Caires and Sterl [23], in which corrections were estimated using a non-parametric method, based on analogues in a learning dataset.

Alternatively, if three or more concurrent datasets are available then a multiple collocation technique can be used to explicitly

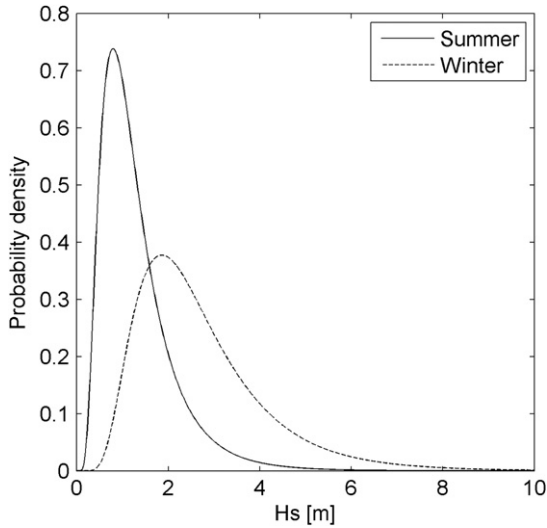


Fig. 1. Summer and winter distributions of  $H_s$  at EMEC.

calculate the bias relative to one dataset and error variance of each dataset [24,25].

Another approach is to compare the distribution functions of modelled and measured parameters via quantile-quantile plots [24,26–29]. Using distribution functions has the advantage that the effects of random errors and temporal offsets (jitter errors) are smoothed out.

#### 4.2. A note on the interpretation of results

In model validation studies, the objective is usually to determine the model response for a given sea state. For the purposes of estimating WEC yield we would like to know what the actual sea state is for a given modelled estimate. These two problems are subtly different. It may seem logical to determine the mean value reported by a buoy for a given model estimate, since this is what we want to know. However, this method will lead to a calibration which is dependent on the distribution of the parameter in interest ( $H_s$  or  $T_e$ ) during the calibration period.

Consider a comparison of  $H_s$  from a model with a buoy. Suppose that the model has normally distributed errors with zero mean and a standard deviation of  $0.2 + 0.1H_s$ . We assume that sampling errors in the buoy data are minimal (a reasonable

assumption for 3 or 6 h averages) and simulate buoy and model data for theoretical summer and winter distributions of  $H_s$ . The distribution in both summer and winter is assumed to be log-normal with a mean of 1.5 m in summer and 3.0 m in winter and a variance  $0.7 \text{ m}^2$  in summer and  $2.0 \text{ m}^2$  in winter. The distributions are shown in Fig. 1.

Fig. 2 shows plots of the mean value of model  $H_s$  binned by buoy  $H_s$ , mean buoy  $H_s$  binned by model  $H_s$  and quantile plots for the summer and winter data. Since the model is unbiased, the mean value of model  $H_s$  binned by buoy  $H_s$  is equal to the buoy  $H_s$  and the line is straight. However, it can be seen that the mean value of the buoy for a given model value differs from summer to winter, with a larger bias for low  $H_s$  in winter and the location at which the lines cross different in summer and winter. Similarly, the shape of the quantile plots is dependent on the distribution of buoy  $H_s$ . This is because the distribution of model  $H_s$  is a convolution of the model error distribution with the true distribution of  $H_s$ . The situation is similar to that described by Tolman [30], in the context of observation errors.

So despite the fact that the model is unbiased and does not change calibration, this example demonstrates that it can appear to change calibration throughout the year. It should be noted that the changes between the summer and winter distributions are much larger than interannual changes in distributions, so the differences would be much smaller if we compared bin-average and q–q plots using data for whole years. However, it will be shown Section 5 that there are actual changes in the performance of the model throughout the year, and these changes should not be confused with the apparent changes shown here.

#### 4.3. The calibration problem

A further problem arises when a calibration is applied to the model data. Again we can consider a simple hypothetical situation to illustrate the problem. Suppose we have a modelled estimate  $X_m$  of a real variable  $X$  and that

$$X_m = X + \varepsilon \tag{1}$$

and

$$\varepsilon \sim N(\mu(X), \sigma^2(X)) \tag{2}$$

where  $\varepsilon$  is a normally distributed error, whose mean and variance are both dependent on  $X$ . Suppose that  $\mu(X)$  and  $\sigma(X)$  are stationary

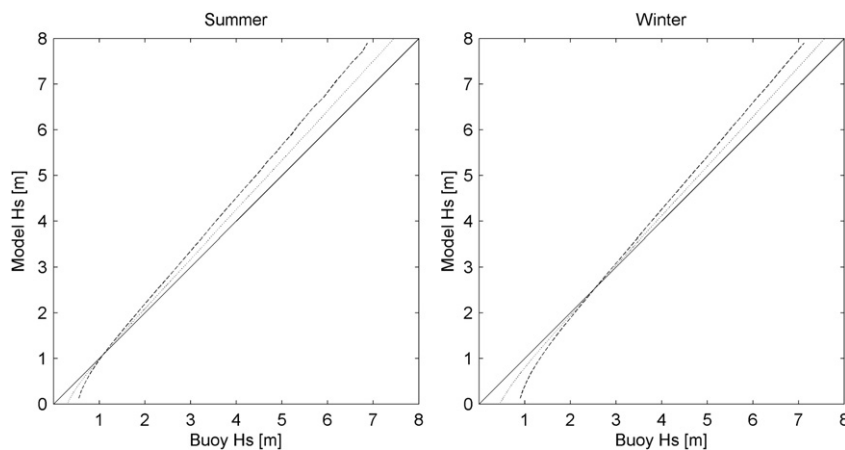


Fig. 2. Solid line: mean model  $H_s$  binned by buoy  $H_s$ ; dashed line: mean buoy  $H_s$  binned by model  $H_s$ ; dotted line: quantile plot. For distributions of  $H_s$  shown in Fig. 1, left – summer; right – winter.

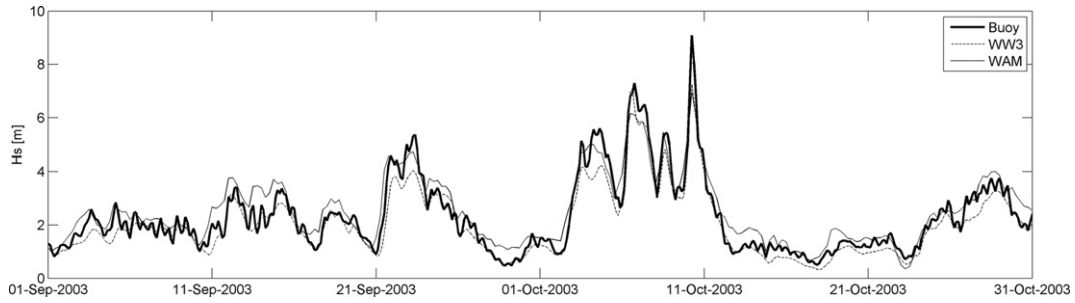


Fig. 3. Time series plots of  $H_s$  from buoy and hindcasts.

in time and can be determined from a bin-average analysis. In this case a functional relationship,  $g$ , can be defined between the real and modelled values:

$$X_m = X + \mu(X) + \delta = g(X) + \delta \quad (3)$$

where

$$g(X) = X + \mu(X) \quad (4)$$

and

$$\delta \sim N(0, \sigma^2(X)) \quad (5)$$

We then calibrate the model by applying the inverse function:

$$Y = g^{-1}(X_m) = g^{-1}(g(X) + \delta) \quad (6)$$

where  $Y$  denotes the calibrated model values. We need to determine whether the mean of the calibrated model,  $Y$ , is equal to the mean of the real variable  $X$ . In the case that  $g$  is a linear function,  $g(X) = aX + b$ , we have  $Y = X + \delta/a$ . So the mean of  $X$  is equal to the mean of  $Y$ , since  $\delta$  has zero mean. However, if  $g$  is non-linear, then the situation is more complicated. For instance if  $g$  is a quadratic function then it is simple to demonstrate that mean value of  $Y$  is not necessarily equal to the mean of  $X$ , the difference being dependent on both the distribution of  $X$  and the error distribution.

If instead we calibrate the model using the mean value of  $X$  for a given  $X_m$ , then by definition the mean values of  $X$  and  $Y$  will be equal within the calibration dataset. However, we are left with the problem that mean value of  $X$  for a given  $X_m$  is dependent on the distribution of  $X$ , so if the distribution of  $X$  changes outside the calibration period then the mean values of  $X$  and  $Y$  will not be equal.

The differences in the mean value of  $X$  and  $Y$  introduced by calibrating using a non-linear function  $g$  are normally quite small.

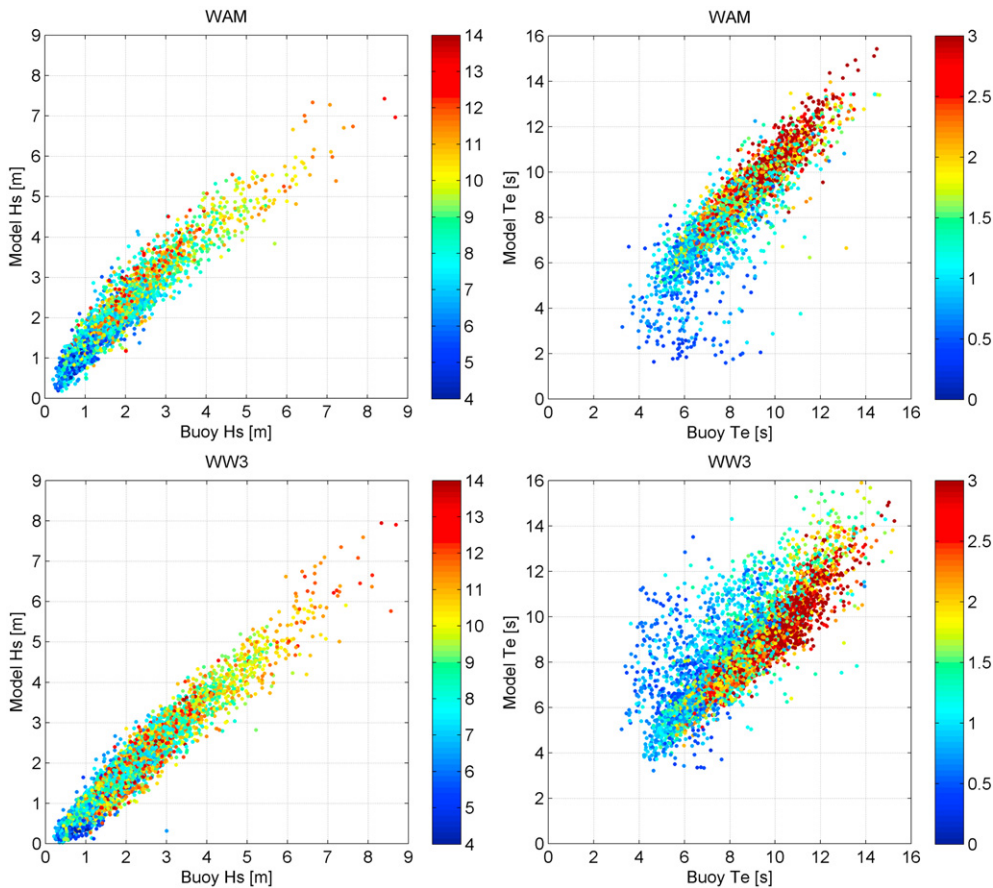


Fig. 4. Scatter plots of buoy and model  $H_s$  (left) and  $T_e$  (right), colour denoting buoy  $T_e$  (left) and buoy  $H_s$  (right).

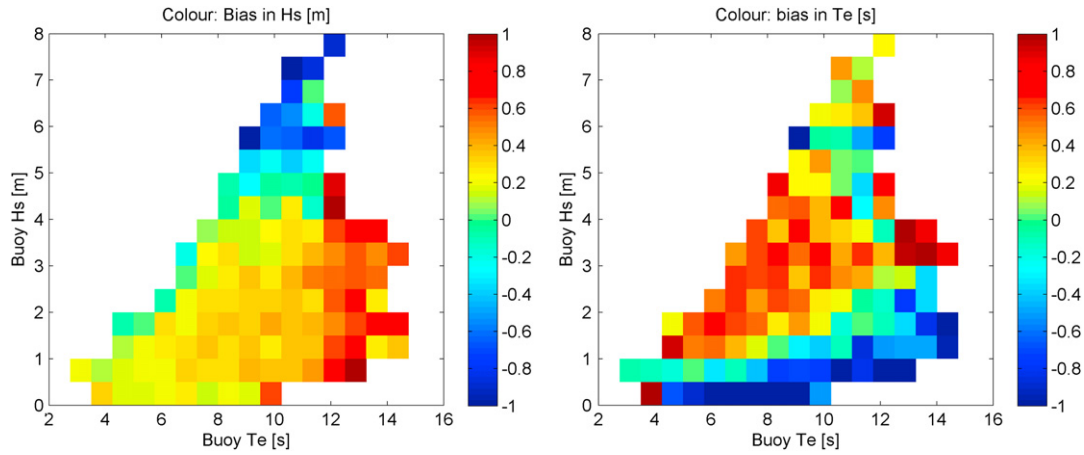


Fig. 5. Bias in  $H_s$  and  $T_e$  for the WAM hindcast binned by buoy  $H_s$  and  $T_e$ .

Moreover, in practice model performance is dependent on multiple parameters, so these arguments become somewhat academic. Nevertheless, they illustrate that some care needs to be taken when determining and applying a calibration to a model.

4.4. Calibration of estimates of WEC power from model data

A number of approaches could be taken to calibrate estimates of WEC power from model data. These include:

*Method A:* Estimates of WEC power from measured and modelled data are compared directly. This approach has the advantage that only one variable is involved. However, the calibration will be dependent on the joint distribution of  $H_s$  and  $T_e$  during the calibration period. For example the power response of a WEC will reach a maximum at some given  $H_s$ , so if the proportion of time that the WEC is operating at maximum power is different outside the calibration period, then a calibration based on model power alone may not be appropriate.

*Method B:* To define a look-up table of the value of WEC power estimated from the buoy, binned by model  $H_s$  and  $T_e$ . This would be a more flexible approach than calibrating by power alone, but suffers from the problems of estimating the mean buoy value for a given model value described in Section 4.2.

*Method C:* To calibrate the model  $H_s$  and  $T_e$  independently, using a bin-average method (binned by buoy values). This method is still

susceptible to problems when applying non-linear calibrations, as described above, but these effects are relatively small. The other point to be aware of is that errors in  $H_s$  and  $T_e$  may be correlated, so adjusting parameters independently may change the shape of the joint distribution and hence estimated WEC power.

This last method will be used in the following section to calibrate the hindcasts for the EMEC test site.

5. Calibration of EMEC hindcasts

5.1. Data

In this section we present an assessment of two independent hindcasts for the EMEC test site, supplied by commercial meteocean consultancies. The first hindcast was produced using the SWAN model [5], with boundary conditions from an archive of operational data from the ECMWF WAM model [16] and covers the period 01/01/1997–31/12/2004 with 6 h time steps. The second hindcast was produced using a nearshore model which accounts for refraction, shoaling and depth induced breaking only, with boundary conditions obtained from a hindcast using WaveWatch III [21]. It covers the period 01/01/92–31/7/2005 with 3 h time steps. The hindcasts will be referred to as the WAM hindcast and the WW3 hindcast. It is stressed that the results should not be interpreted as applicable to WAM or WaveWatch III in general,

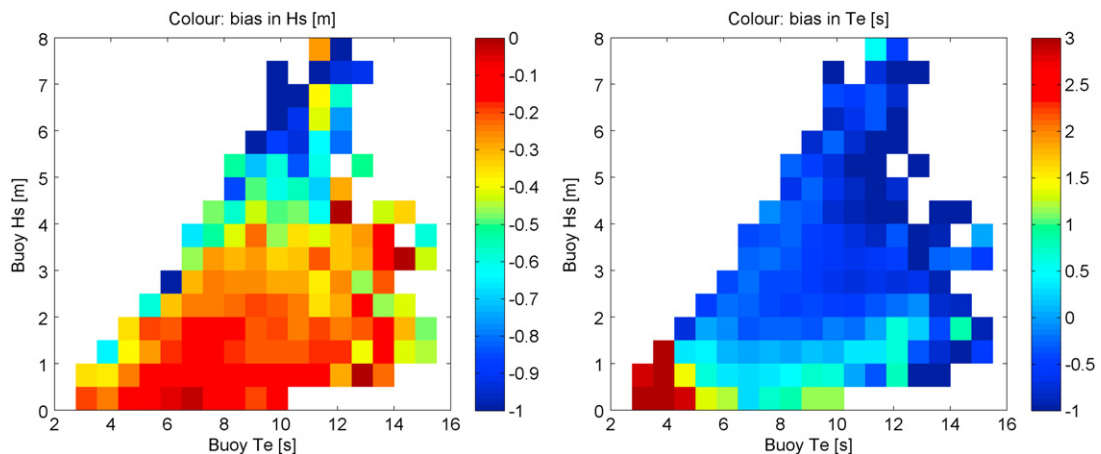


Fig. 6. Bias in  $H_s$  and  $T_e$  for the WW3 hindcast binned by buoy  $H_s$  and  $T_e$ .

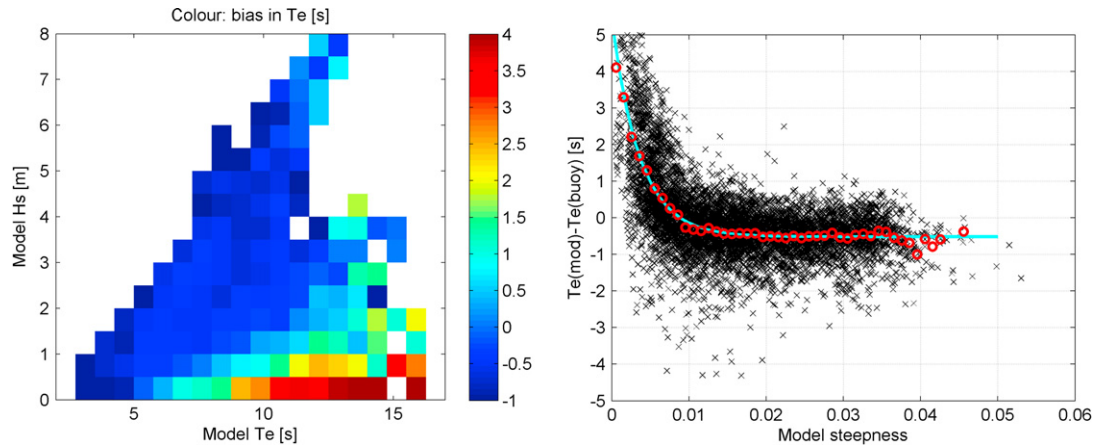


Fig. 7. Left: bias in WW3  $T_e$ , binned by model  $H_s$  and  $T_e$ . Right: bias in WW3  $T_e$  against WW3 steepness. Black crosses: individual points; red circles: bin-average; cyan line: fitted exponential curve.

since we are not attempting to separate the errors introduced by the nearshore models from the errors in the offshore data. Moreover, the data used here is only for one location and the performance of the models can be expected to vary with location. The examination of the hindcast data presented here is intended to illustrate the type of errors which can occur and how they should be treated when estimating WEC yield.

The hindcasts are compared to measurements from a Datawell Directional Waverider buoy moored in 50 m water depth at the EMEC site. Buoy measurements at EMEC began in October 2002 and run until the end of the hindcasts with some missing data. For the comparison with the WW3 hindcast the buoy data has been averaged to give 3 h values and for the comparison with the WAM hindcast it has been averaged to 6 h values. The nearshore models are assumed to be of sufficiently high spatial resolution that spatial variability is not significant. However, since the input data for the nearshore models comes from global scale models, this assumption is slightly unrealistic. The buoy measurements of  $H_s$  have a sampling variability of about 2% for a 3 hour average and about 1% for a 6 h average (sampling variability of wave measurements is discussed in [31–34]). Since the errors in the modelled data are much larger than this, it can be inferred from the results of Tolman [30] that this level of sampling variability will have negligible impact on our results.

5.2. Analysis of trends in the models

The first step in assessing the hindcasts is to examine the time series. Fig. 3 shows plots of  $H_s$  from the models and the buoy over a two-month period. The trends shown here are representative of whole calibration period. On the whole, the models seem to reproduce the time series of  $H_s$  quite well and temporal offsets appear small. The estimate of  $H_s$  from the WW3 hindcast is consistently lower than the buoy data and the estimate from the WAM hindcast is consistently higher, although both models underestimate the most intense storm in this period. A 3 h average of buoy data has been used in this plot, but it is clear that there is still more short-term variability in the buoy data than in the WW3 data. This is mainly because the nearshore model data is based on estimates from large-scale models which will give smoother time series. Also there is evidence of tidal modulation of the waves in the buoy data, and tidal current effects were not included in either model.

The next step is to examine scatter plots of the parameters. Fig. 4 shows scatter plots of model  $H_s$  against buoy  $H_s$  and model  $T_e$  against buoy  $T_e$ . It is instructive to colour the plots by the buoy  $H_s$  and  $T_e$ , to see if the performance of model  $H_s$  is dependent on buoy  $T_e$  or model  $T_e$  on buoy  $H_s$ . The scatter is reasonably low for  $H_s$ , but it is visible that the WAM hindcast tends to overestimate  $H_s$  between

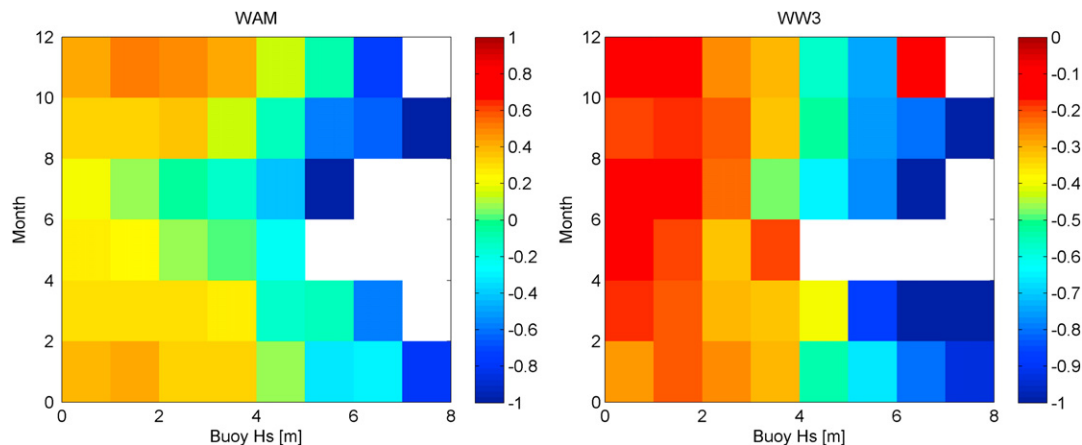


Fig. 8. Bias in hindcast  $H_s$  binned by month and buoy  $H_s$ .

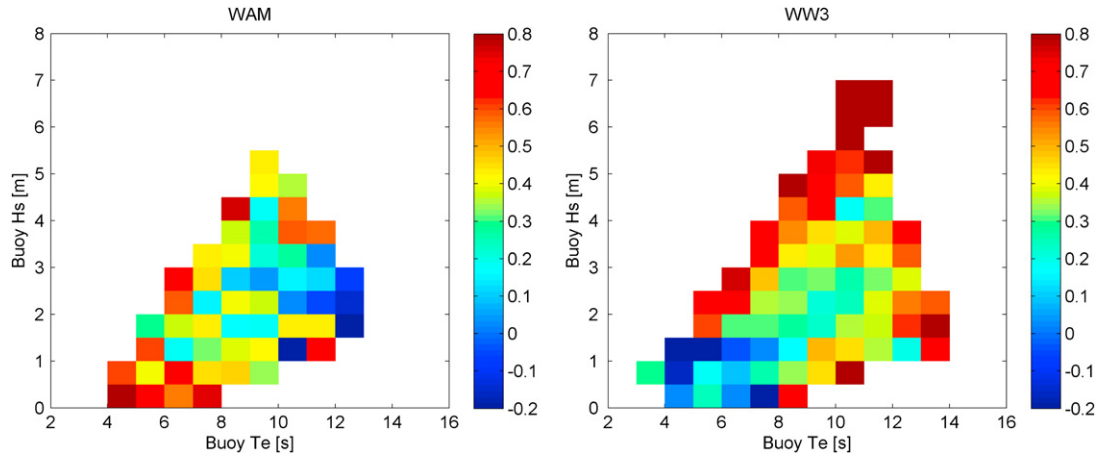


Fig. 9. Correlation of errors in model  $H_s$  and  $T_e$  binned by buoy  $H_s$  and  $T_e$ .

2 m and 4 m at longer periods. For both hindcasts there is more scatter for  $T_e$ , especially for low  $H_s$ .

Fig. 5 shows the bias in the WAM hindcast, binned by buoy  $H_s$  and  $T_e$ . As was seen in the scatter plots, the WAM hindcast is observed to over-predict  $H_s$  to a greater extent for swell events, where  $T_e > 12$  s and  $H_s < 5$  m. This counts for less than 5% of our dataset, and for the remaining data the bias in  $H_s$  appears to be dependent on  $H_s$  only. The poor performance of model  $T_e$  in low  $H_s$  is also clear. A trend is observed with buoy steepness, but not with model steepness, and is therefore difficult to correct for. Since the poor performance occurs at low  $H_s$  and hence low WEC power, no attempt is made to correct for it and instead only

points with buoy  $H_s > 1$  m are used to calibrate  $T_e$  from the WAM hindcast. However, although these data are not used in the calibration of  $T_e$ , they are used for the assessment of the derived WEC power.

Fig. 6 shows similar plots for the WW3 hindcast. The dependence of the error in model  $H_s$  on buoy  $T_e$  does not appear to be as strong as for the WAM hindcast. There is some trend visible in the error in model  $T_e$  on buoy  $H_s$ . However, if the performance of WW3  $T_e$  is examined in terms of model parameters the trend is much stronger. Fig. 7 shows the bias in model  $T_e$  against model  $H_s$  and  $T_e$ , and also against model steepness (here steepness is defined in terms of  $T_e$  rather than the usual definition based on  $T_z$ , as steepness

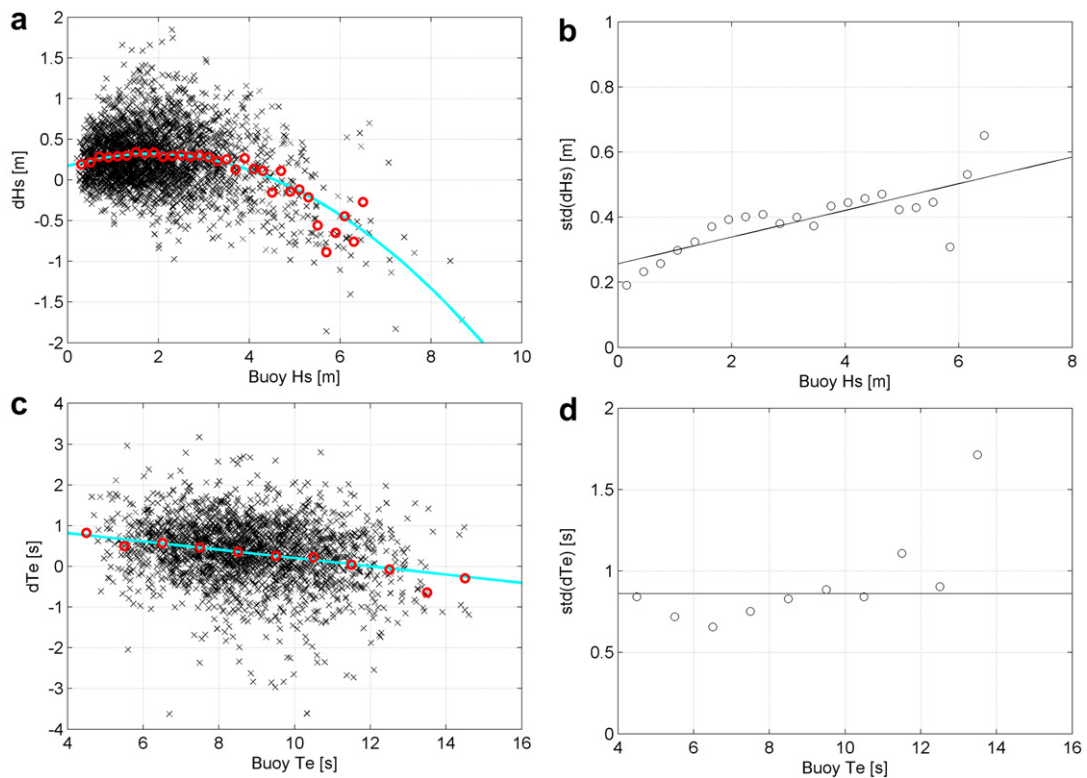


Fig. 10. Calibration plots for the WAM hindcast. (a) Error in model  $H_s$  against buoy  $H_s$ . Black crosses: individual points; red circles: bin-average; cyan line: fitted quadratic curve. (b) Standard deviation of error in model  $H_s$ . Circles: bin-average; line: fitted linear relationship. (c) Error in model  $T_e$  against buoy  $T_e$ , for buoy  $H_s > 1$  m. Black crosses: individual points; red circles: bin-average; cyan line: fitted linear relationship. (d) Standard deviation of error in model  $T_e$ . Circles: bin-average; line: average over dataset.

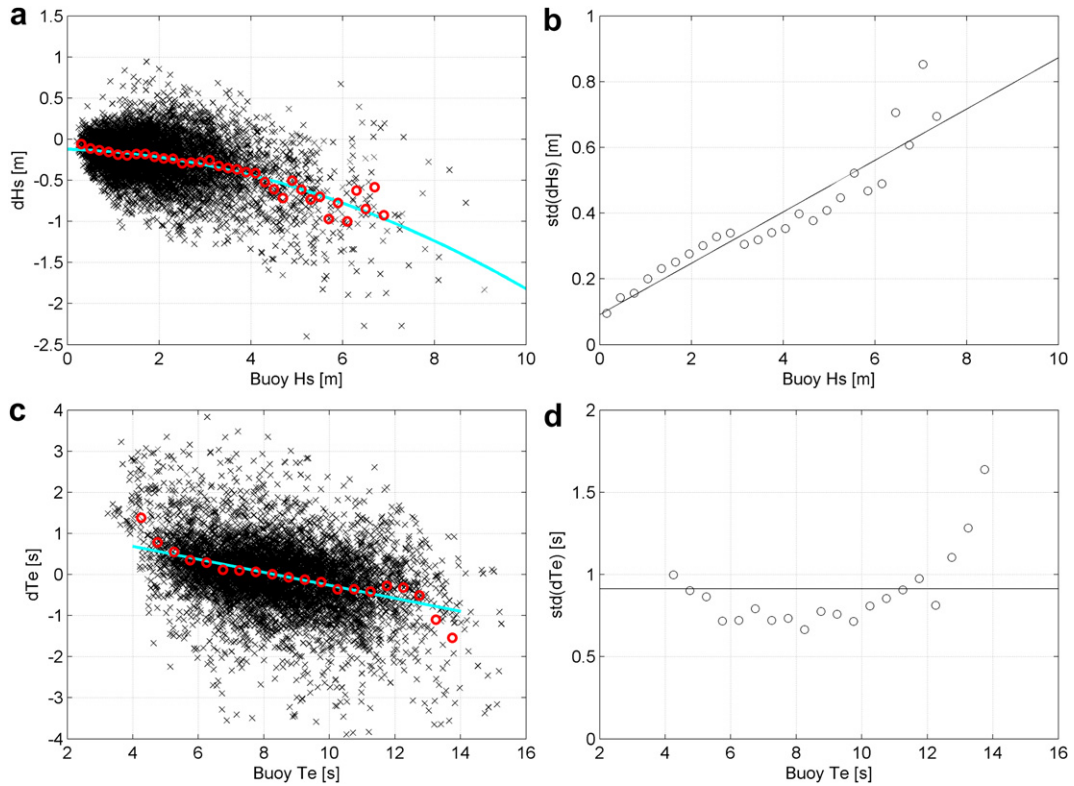


Fig. 11. As previous figure, but for the WW3 hindcast.

$= 2\pi H_s / g T_e^2$ ). The model is effectively over-predicting  $T_e$  for low-steepness swell events. A new model period is defined, with an exponential correction in steepness (shown in Fig. 7). From hereon this definition is used for WW3  $T_e$ .

This correction in terms of model parameters is subject to the effects of changing distributions, discussed in the last section. However there is little that can be done about it, since the trend is not evident with buoy parameters. The correction is also remarkably effective in decreasing the level of scatter, with the standard deviation of the differences decreasing from 1.17 s for the original data to 0.85 s for the new definition.

The dependence of model errors on direction was tested for, but no trend was found. The performance of both hindcasts is likely to be dependent on numerous other factors, such as frequency, swell age, wind sea component, etc. However, in this example we only consider dependence on  $H_s$  and  $T_e$ . Strictly speaking, it is only fair to assume that model errors are purely random when there is no residual dependence on other factors.

Fig. 8 shows how the bias in model  $H_s$  changes throughout the year. The WAM hindcast over-predicts low  $H_s$  in the winter, but is almost unbiased at low  $H_s$  in the summer. This is contrary to the results of Janssen [19] who showed that when results were

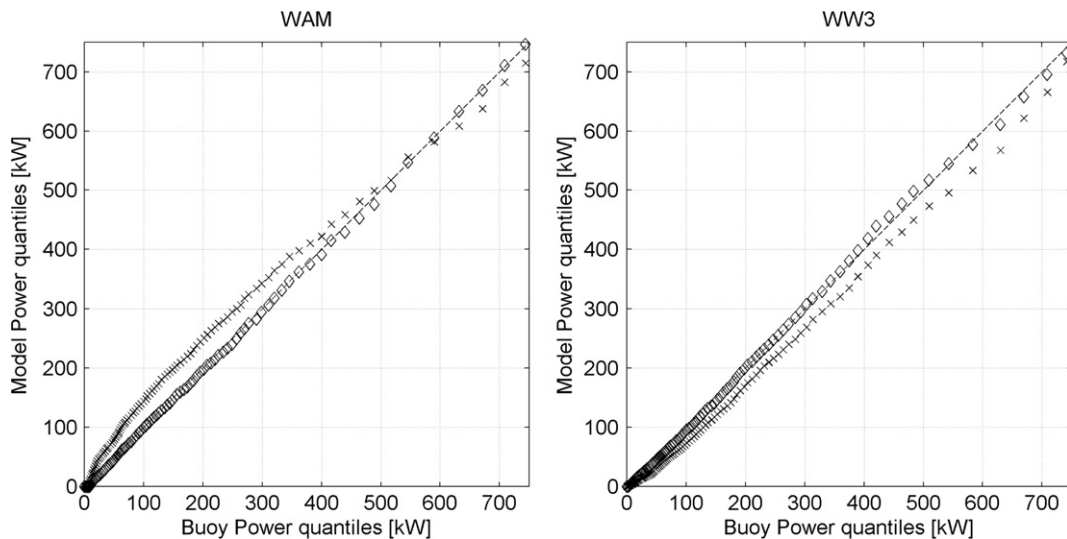


Fig. 12. Quantile plots of hindcast against buoy Pelamis power. Crosses: uncalibrated values; diamonds: calibrated.

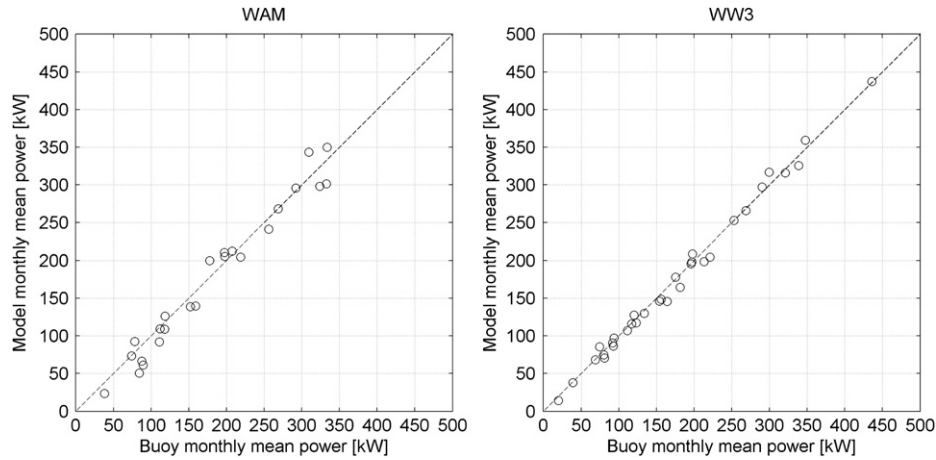


Fig. 13. Scatter plots of monthly mean Pelamis power for calibrated hindcasts against buoy values.

averaged over a number of buoys the ECMWF WAM model overestimates low frequency energy in the summer. Since we are binning by  $H_s$  rather than frequency, our results are not directly comparable, but the changing bias observed here may be a result of the tuning of the model to compensate for biases elsewhere. Note that since we are binning results by buoy parameters, the changing calibration is not a result of changing distributions between summer and winter, described in Section 4.2. The WW3 hindcast does not appear to perform differently in summer and winter, despite the shorter colour scale used in the plot.

Finally, we can test for correlation of the errors in  $H_s$  and  $T_e$ . Overall the correlation is low, about 0.2 for the WAM hindcast and 0.1 for the WW3 hindcast. However, errors in certain sea states are more strongly correlated. Fig. 9 shows the correlation of errors in model  $H_s$  and  $T_e$ , binned by buoy  $H_s$  and  $T_e$ . Note that only bins containing 10 or more points have been displayed. For the WAM hindcast a stronger correlation is apparent for low  $H_s$ , which may be related to the poor performance of model  $T_e$  at low  $H_s$ . For the WW3 hindcast the correlation in the errors is strongest in steep seas. This is a result of the limiting steepness of ocean waves, which necessitates that an increase in  $H_s$  for a steep sea is accompanied by an increase in period. There is also some positive correlation of errors in swell events. However, for the highest occurrence sea states the correlation is low.

### 5.3. Calibration of the hindcasts

The hindcasts are calibrated using separate corrections for  $H_s$  and  $T_e$ , determined from a bin-average analysis. A seasonal calibration for the WAM data was tested and found to perform worse

outside the calibration period, than a non-seasonal adjustment. This is thought to be because calibrating for each season reduces the number of points and therefore increases the uncertainty in estimating trends. Figs. 10 and 11 show bin-average plots of the bias and standard deviation in the model errors. We model the bias in  $H_s$  as quadratic, and the bias in  $T_e$  as linear. The standard deviation is modelled as linear in  $H_s$  and constant in  $T_e$ . At higher values of  $H_s$  and  $T_e$  there are few data points, which makes the estimates of the standard deviation of the errors uncertain. Therefore the points which are away from the trend lines on the far left of Figs. 10(b), (d) and 11(b), (d) are not considered significant.

The use of a quadratic calibration for  $H_s$  means that there will be a maximum model response at some point. For the WAM hindcast this occurs when the buoy  $H_s$  is 13.2 m and model  $H_s$  is 7.9 m. Clearly this is not a realistic assumption, since the WAM hindcast contains storms outside the calibration period, exceeding this value, with a maximum of 8.4 m. The situation is not as severe for the WW3 model, with the maximum occurring when the buoy  $H_s$  is 32.3 m and model  $H_s$  is 15.7 m. This does not present a problem for the estimation of WEC power, but clearly is not satisfactory for the estimation of extremes.

Fig. 12 shows quantile plots of Pelamis power for the calibrated and uncalibrated models against values from the buoy. The Pelamis power has been calculated from the power matrix shown in Table 1 interpolated to a resolution of 0.1 m  $H_s$  and 0.1 s  $T_e$ . There is a clear improvement for both models after calibration, but with some small discrepancies remaining. This is most likely because the parametric correction that was applied does not entirely describe the model behaviour. But it could also be a result of correlation in the errors in  $H_s$  and  $T_e$  or an effect of using a non-linear calibration,

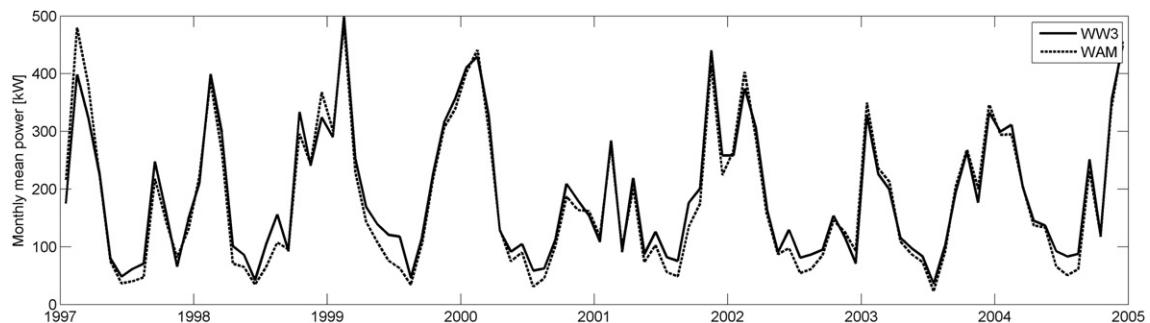


Fig. 14. Monthly mean Pelamis power from the calibrated hindcasts.

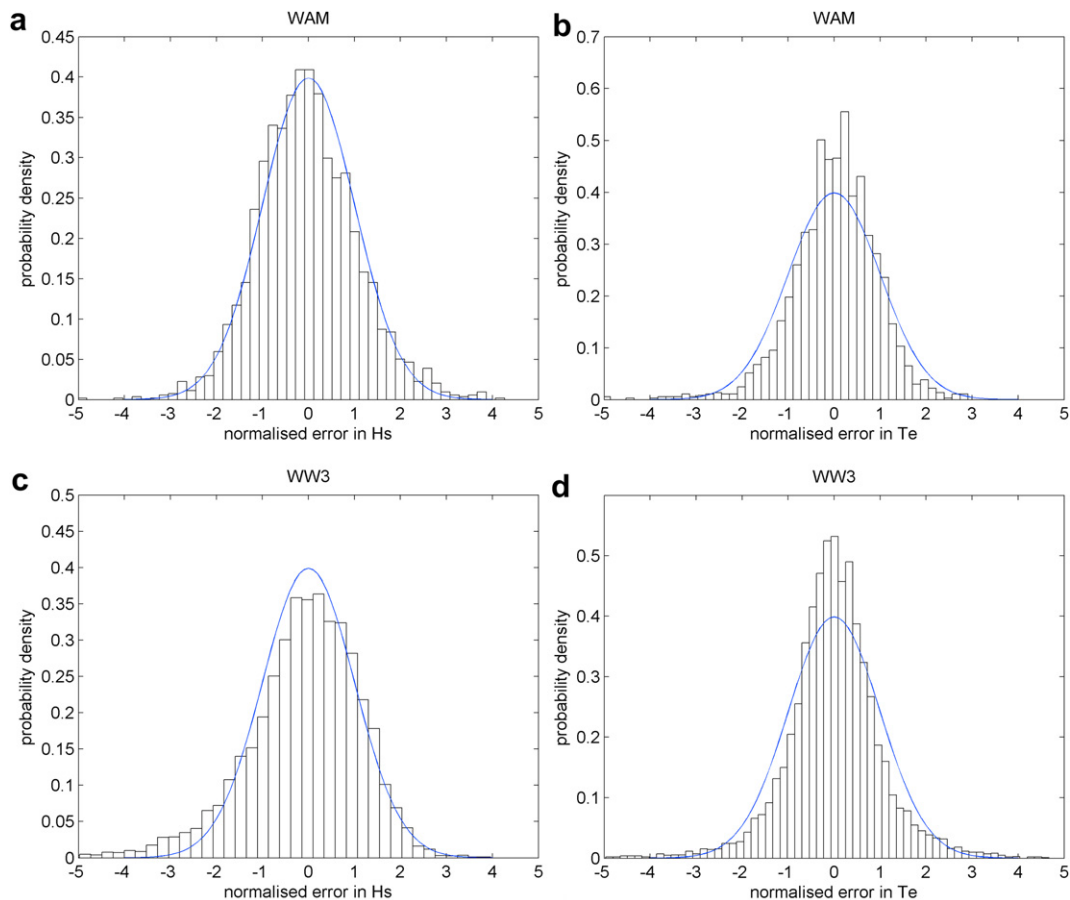


Fig. 15. Distribution of normalised errors in model  $H_s$  and  $T_e$  (histograms) with fitted normal distribution (lines).

described in Section 4.3. Considering the models are calibrated in terms of  $H_s$  and  $T_e$  and the Pelamis response is calculated afterwards, the result is good. For the WAM hindcast, the bias before calibration is 30.1 kW and  $-4.0$  kW after calibration. For the WW3 hindcast, the bias before calibration is  $-24.4$  kW and  $-2.3$  kW after calibration. Fig. 13 shows scatter plots of monthly mean Pelamis power for the calibrated models against buoy values. It is clear that the agreement is better for the WW3 model. The standard deviation is 18.1 kW for the WAM hindcast and 7.9 kW for the WW3 hindcast.

Fig. 14 shows the monthly mean Pelamis power from calibrated hindcasts for the 8-year period that they overlap. The mean power over the entire period is 188.4 kW for the WW3 hindcast and 179.4 kW for the WAM hindcast, a difference of 5%, compared with 167.9 kW and 212.9 kW before calibration. This is an improvement, but it is clear from Fig. 14 that some residual trends remain. In particular the calibrated WAM hindcast gives consistently lower powers in the summer months, a consequence of the seasonal change in calibration mentioned before. Moreover, since the boundary conditions for the WAM hindcast came from an archive of operational data from the ECMWF WAM model, changes to the operational model made over the years are likely to affect the calibration.

There are also some differences during the calibration period. The calibrated WAM hindcast is lower than the WW3 hindcast during the period June–August 2004. However, the agreement in the previous summer (also within the calibration period) was good. The calibrated WW3 hindcast is in much closer agreement with the buoy during June–August 2004, so this provides further evidence of changing biases in the WAM hindcast.

## 6. Estimation of confidence bounds on mean WEC power

The error in the estimate of Pelamis power from each model exhibits correlation over short time scales. This suggests the use of time series models for representing the evolution of errors and estimating confidence bounds for the estimates of power from the hindcasts. The magnitude of the error in WEC power is related to the wave conditions at the time, so this dependence must be removed before the time series model is fitted. The procedure we will follow to fit the time series model consists of the following steps:

- Estimate distributions of errors in hindcast  $H_s$  and  $T_e$
- Calculate the distribution of errors in hindcast WEC power.
- Normalise the error in hindcast power.
- Fit time series model

To estimate confidence bounds we can then generate a large number of simulations of the normalised error in hindcast power using the fitted time series model. We then un-normalise to get a number of simulated realisations of the error in power over the entire hindcast. From this we can calculate error bounds for monthly, annual or multi-year averages of WEC power.

Fig. 15 shows the distribution of the errors in the calibrated hindcast  $H_s$  and  $T_e$ , normalised by the standard deviations (shown in Fig. 10 and 11). The normalised errors are approximately normally distributed, apart from WW3  $T_e$  which shows a slightly more peaked distribution. However, we will approximate this with a Gaussian.

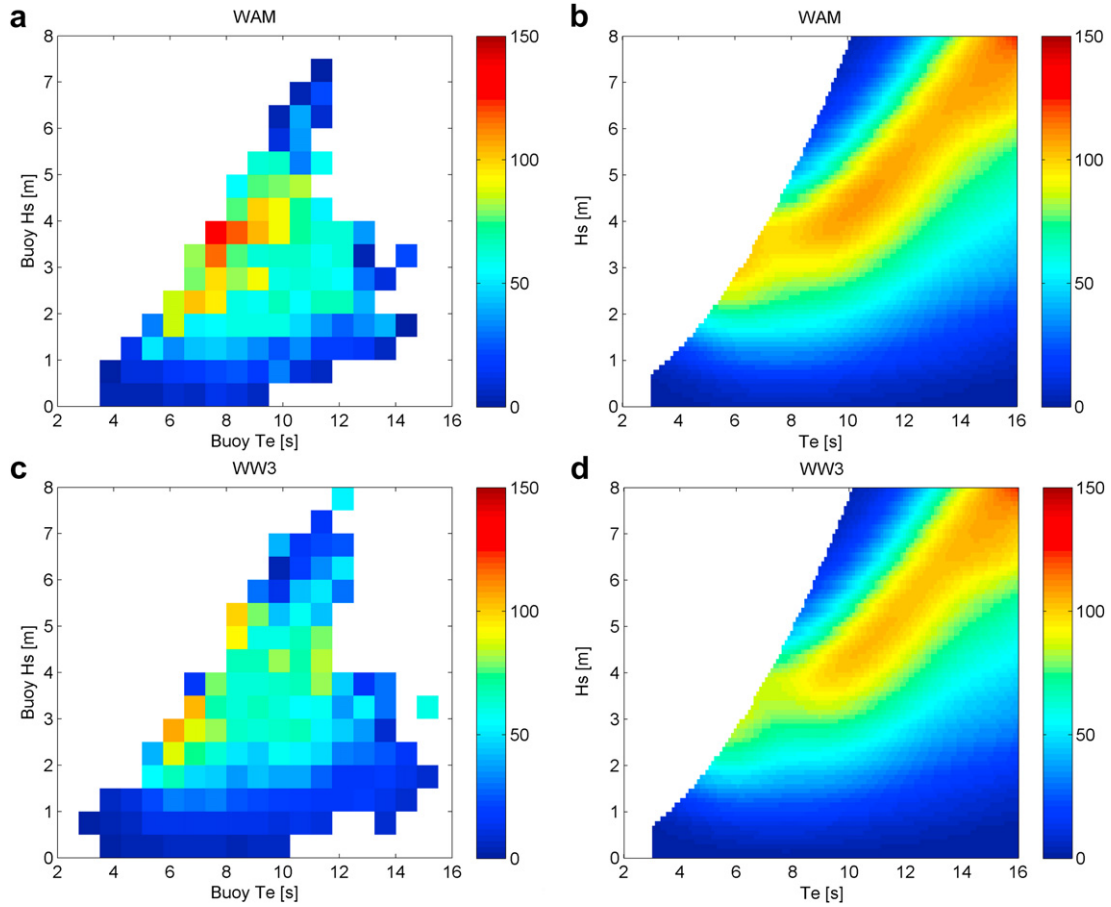


Fig. 16. Standard deviation of the error in model power for WAM (top) and WW3 (bottom). Left: from equation (7). Right: from equation (8).

The error in model estimates of Pelamis power is a function of both  $H_s$  and  $T_e$ . Fig. 16(a) and (c) show the standard deviation of the error in model power, binned by the buoy values of  $H_s$  and  $T_e$ . This can be written formally as follows: let  $H_b(t_i)$  and  $T_b(t_i)$  denote the buoy measurements at time  $t_i$ , and  $H_m(t_i)$  and  $T_m(t_i)$  denote the model estimates. Let  $P(H, T)$  denote the Pelamis power response calculated by linearly interpolating the values shown in the power matrix (Table 1). If we define the set  $S$  as all values of  $i$  such that  $H_s -$

$dh/2 \leq H_b(t_i) < H_s + dh/2$  and  $T_e - dt/2 \leq T_b(t_i) < T_e + dt/2$ , then the values shown in Fig. 16(a) and 16(c) are given by

$$\sigma(H_s, T_e) = \sqrt{\sum_{i \in S} [P(H_m(t_i), T_m(t_i)) - P(H_b(t_i), T_b(t_i))]^2} \quad (7)$$

In Fig. 16 a bin size of  $dh = 0.5$  m and  $dt = 0.75$  s has been used. The bin size is a compromise between adequate resolution and

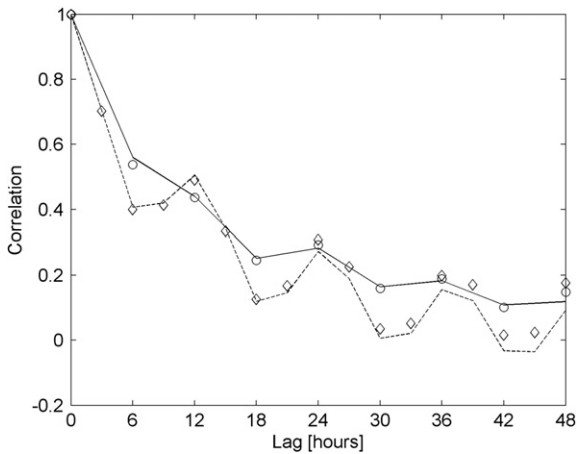


Fig. 17. Auto-correlation series of normalised errors. Circles and solid line: values for WAM hindcast and fitted ARMA (2,3) model. Diamonds and dashed line: values for WW3 hindcast and fitted ARMA (3,2) model.

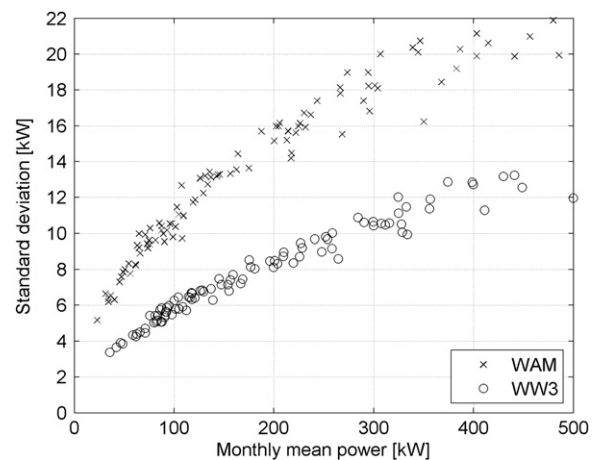


Fig. 18. Standard deviation of the error in monthly mean power from the ARMA simulations against estimated monthly mean power from the hindcasts.

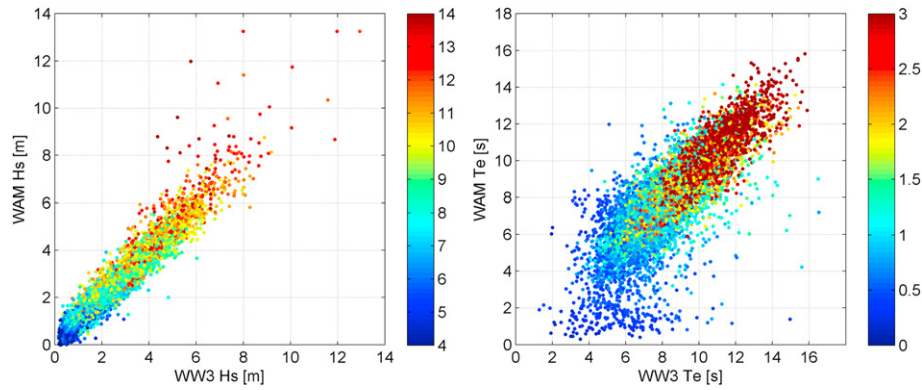


Fig. 19. Scatter plots of  $H_s$  coloured by  $T_e$  (left) and  $T_e$  coloured by  $H_s$  (right) for the calibrated hindcasts.

having enough data to accurately estimate the standard deviation. The standard deviation of the error in model power can also be calculated from the estimates of the error distributions of model  $H_s$  and  $T_e$ . The model errors in  $H_s$  and  $T_e$  are correlated in some places, so strictly this should be accounted for when calculating the distribution of the error in estimated Pelamis power. However, it was found that accounting for the correlation made little difference in practice and they are assumed to be independent here. Let  $f_{H_m|H_s}$  and  $f_{T_m|T_e}$  denote the density functions of the model values of  $H_s$  and  $T_e$ , given the real values. The pdf  $f_{H_m|H_s}$  is modelled as normal with standard deviation increasing linearly with  $H_s$ , and the pdf  $f_{T_m|T_e}$  is modelled as normal with constant standard deviation (see Figs. 10 and 11). Then the variance of the model power for a given  $H_s$  and  $T_e$  is given by

$$\sigma^2(H_s, T_e) = \int_0^\infty \int_0^\infty f_{H_m|H_s}(h_m) f_{T_m|T_e}(t_m) [P(h_m, t_m) - P(H_s, T_e)]^2 dh_m dt_m \quad (8)$$

Fig. 16(b) and (d) show the standard deviation of model error calculated using equation (8). The agreement with the values calculated from equation (7) is good, indicating that approximations which have been used for  $f_{H_m|H_s}$  and  $f_{T_m|T_e}$  are reasonable. This method of calculating the model error in Pelamis power has the advantage that the resolution can be made as high as required, so that the standard deviation can be calculated more precisely for a given  $H_s$  and  $T_e$ . This method will be used to normalise the errors in hindcast power.

If the uncertainty in WEC response were known, it could be factored in at this point. As was discussed in Section 1, a WEC will likely have a range of responses for a given  $H_s$  and  $T_e$  due to variation in spectral shape and directional distribution. We define  $Q$  to be the actual power generated by a WEC in a given sea state, and the probability that  $Q=q$ , given that  $H_s=h$  and  $T_e=t$ , as  $f_{Q|H_s, T_e}(q)$ . The distribution  $f_{Q|H_s, T_e}$  will typically vary from site to site, depending on the distribution of different spectral shapes which occur for a given  $H_s$  and  $T_e$ . Suppose that  $f_{Q|H_s, T_e}$  is known for the site in question, then equation (8) can be modified to include this additional level of uncertainty, by integrating over the range of possible powers for a given  $H_s$  and  $T_e$ :

$$\sigma^2(H_s, T_e) = \int_0^\infty \int_0^\infty \int_0^\infty f_{H_m|H_s}(h_m) f_{T_m|T_e}(t_m) f_{Q|H_s, T_e}(q) [P(h_m, t_m) - q]^2 dh_m dt_m dq \quad (9)$$

where, as before,  $P(H, T)$  is defined to be the power specified in the power matrix.

Returning to the time series modelling, since the error in hindcast power is dependent on  $H_s$  and  $T_e$ , the errors need to be normalised before fitting a time series model. Each error in hindcast power is divided by the standard deviation calculated from the estimated distributions of errors in model  $H_s$  and  $T_e$  (the right hand plots in Fig. 16). The resultant distribution of normalised errors is slightly non-Gaussian so we use the transformation:

$$z = \Phi^{-1}(F_X(x)) \quad (10)$$

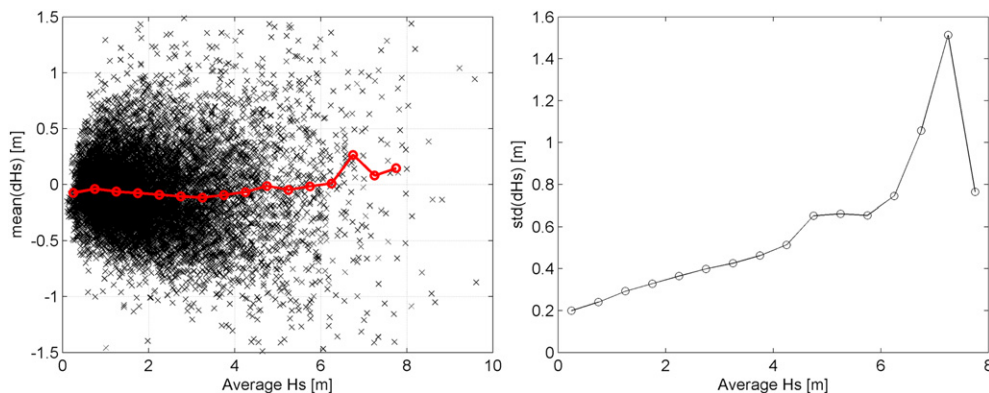


Fig. 20. Mean and standard deviation of differences in  $T_e$  between calibrated models, for average  $H_s > 1$  m.

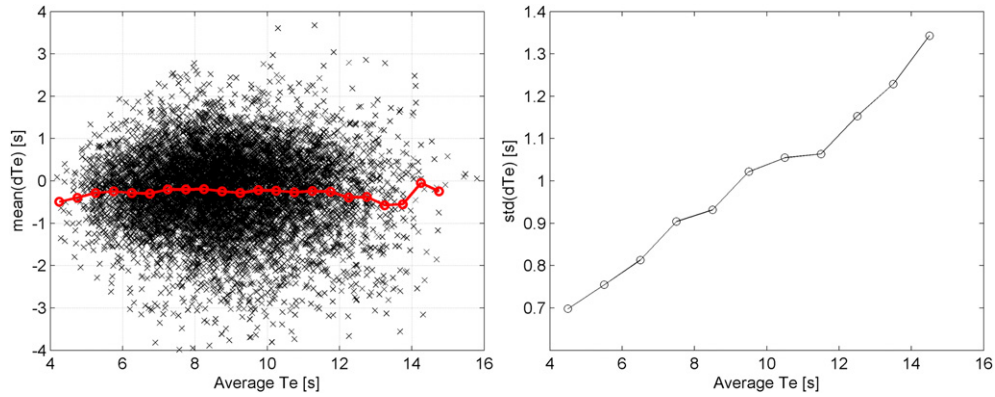


Fig. 21. Mean and standard deviation of differences in  $H_s$  between calibrated models.

where  $\Phi$  is the distribution function of the standard normal distribution and  $F_x$  is the empirical distribution function of  $X$ . This transformation forces the empirical distribution of  $z$  to be exactly Gaussian.

Auto-regressive moving-average (ARMA) models are fitted to the normalised errors in power using the method described in [35]. The order of the model is chosen by minimising Akaike's Information Criterion. An ARMA (2,3) model was found to provide the best fit for the WAM residuals and an ARMA (3,2) was found to give the best fit for the WW3 residuals. Fig. 17 shows the auto-correlation series for the errors in normalised hindcast power and the fitted ARMA model. It is clear that both ARMA models are in good agreement with the observed auto-correlations. The error caused by the tidal modulation of the wave field is also clearly visible. It is less pronounced for the WAM hindcast because of 6 h averages are used instead of 3 h averages for the WW3 hindcast. When the WW3 hindcast was averaged to give 6 h values, the auto-correlation series was very close to that for the WAM hindcast.

To estimate confidence bounds for the calibrated hindcasts the following procedure is followed:

- Generate 1000 ARMA simulations, the same length as the hindcast.
- Apply the inverse transformation of equation (10).
- Multiply by the standard deviation of the error in model power obtained from the look-up table shown in Fig. 16 (right hand plots).

Note that here we are substituting the standard deviation in error for a given calibrated model estimate, for the standard deviation for a given buoy value. However, comparison of the two distributions showed that they are very similar.

Fig. 18 shows a scatter plot of the standard deviation of the error in monthly mean power from the ARMA simulations against estimated monthly mean power from the calibrated hindcasts. The WAM hindcast has higher monthly errors due to slightly higher error in individual estimates. The relationship between monthly mean power and the standard deviation in the model estimate is slightly non-linear, with the gradient decreasing with higher monthly mean power. This is because when monthly mean power is high there is a high proportion of time when the Pelamis is operating at maximum power, and the standard deviation of the model estimate is lower.

The differences between the monthly mean power from the buoy and calibrated WW3 hindcast (see Fig. 13) fall within the 95% limits obtained from the ARMA simulations, but the monthly errors from the calibrated WAM hindcast are not within the range from the ARMA simulations. This is likely to be due to the changing seasonal calibration, which it was not possible to capture with the low-order ARMA model.

The 95% confidence interval for the mean power over the 8 year period from the ARMA simulation, is  $\pm 1.6$  kW for the WW3 hindcast and  $\pm 3.0$  kW for the WAM hindcast. The actual difference in the 8-year mean power is 9.0 kW, outside the predicted bounds from the ARMA simulations. Moreover, in 24 of the 96 months that the hindcasts overlap, the differences between the monthly mean

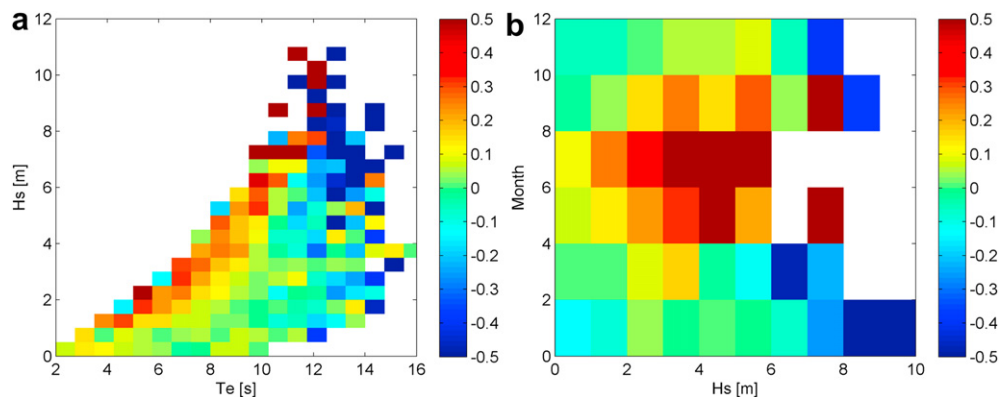


Fig. 22. (a) Mean difference in  $H_s$ , binned by  $H_s$  and  $T_e$ . (b) Mean difference in  $H_s$ , binned by  $H_s$  and month.

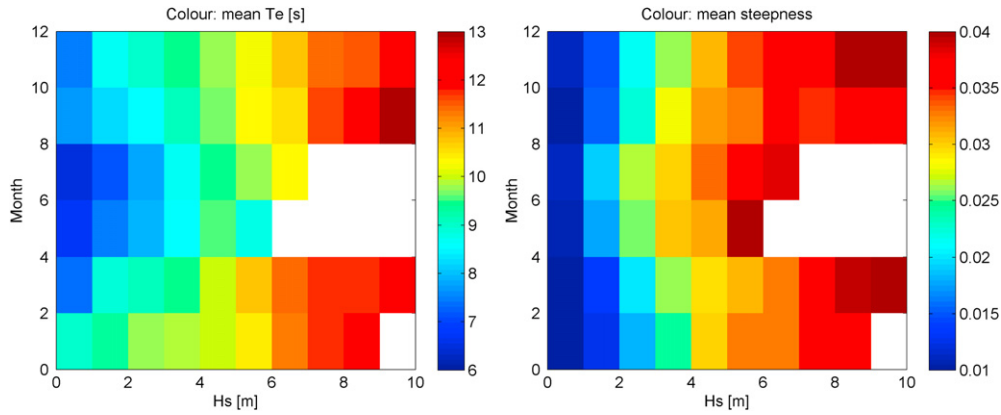


Fig. 23. Mean  $T_e$  (left) and steepness (right) binned by  $H_s$  and month, from 5 years of EMEC buoy data.

values are outside the 95% bounds from the combined ARMA models. We have already seen that the ARMA model does not capture the uncertainty from changing seasonal calibration in the WAM hindcast during the calibration period, and it will not account for any changes to the ECMWF operational WAM model outside this period.

The bias in the mean power from the calibrated WW3 hindcast over the 2 year calibration period was  $-2.3$  kW and the 95% bounds from the ARMA simulations are  $\pm 3.4$  kW. So it is possible that the ARMA model is a valid representation of the uncertainty for the WW3 hindcast, seeing as errors for individual months were also within the bounds from the ARMA model. However, it is possible that there could be some component of bias which is not captured by the ARMA model (which represents a zero-mean random process) which may affect the accuracy outside the calibration period.

### 7. Comparison of calibrated hindcasts

To help understand the reasons for the differences between the two hindcasts, we can compare the calibrated data. Fig. 19 shows scatter plots of  $H_s$  and  $T_e$  for the calibrated hindcasts. It is clear that there is still some residual dependence of  $H_s$  on  $T_e$  and vice versa. The disagreement in  $T_e$  between the two models at low  $H_s$  is not surprising, since we ignored points with  $H_s < 1$  m for the calibration of the WAM hindcast. If these points are removed, the agreement is good. Fig. 20 shows the mean and standard deviation of differences between calibrated  $T_e$ , for average  $H_s > 1$  m. There is a small bias of 0.25 s which seems constant over the entire dataset. The standard deviation of the differences in  $T_e$  increases approximately linearly with  $T_e$ . This trend was not so evident in the comparisons with the buoy, since there were fewer data points.

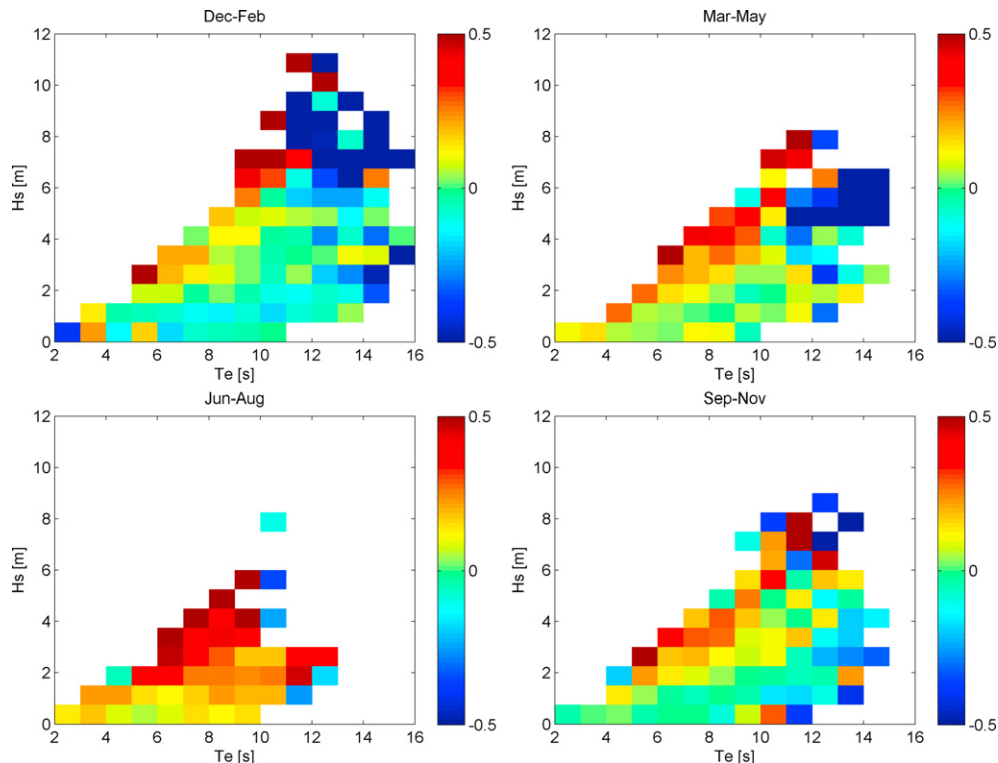


Fig. 24. Seasonal mean difference in  $H_s$  between the calibrated models, binned by  $H_s$  and  $T_e$ .

For  $H_s$  the dependence on period is consistent with the trend observed between the WAM hindcast and the buoy. There is a much larger disagreement between the models at high  $H_s$ . From inspection of the time series, it is clear that this is not a result of jitter errors, but differences in the estimation of the peak  $H_s$  in a storm. This disagreement is not so important for estimating WEC power, but is much more serious for the analysis of extremes. Fig. 21 shows the mean and standard deviation of differences in  $H_s$  between the calibrated hindcasts. There is a small bias of 7 cm over the entire hindcast, but which varies slightly with  $H_s$ . The standard deviation in the differences increases linearly with  $H_s$  up to about 6 m, at which point it increases sharply due to the increased uncertainty in large storms.

Fig. 22(a) shows the mean difference in  $H_s$ , binned by  $H_s$  and  $T_e$ . It is clear that the WW3 hindcast gives higher estimates in steep seas and lower estimates at longer periods. The tendency for the WAM hindcast to over-predict at longer periods was evident in the buoy data, but a trend with steepness was not evident for either model. Fig. 22(b) shows the mean difference in  $H_s$ , binned by  $H_s$  and month. There are clear seasonal changes in the differences. The trend observed is consistent with that observed between the WAM hindcast and the buoy.

From the buoy data we know that there are seasonal changes in the mean  $T_e$  and steepness for a given  $H_s$ , with storms in summer generally steeper than those in winter (see Fig. 23). However, these changes are not wholly responsible for the differences in calibration. Fig. 24 shows the mean difference in  $H_s$  between the calibrated models, binned by  $H_s$  and  $T_e$ , broken down into 4 seasons. It is clear that the dependence on steepness varies with season. This could be due to seasonal changes of parameters we are not considering, such as swell age, mean direction, or directional spread. Alternatively it could be due to seasonal changes in conditions over the whole model domain, causing different amounts of error to occur and propagate through the model to the EMEC site.

## 8. Discussion and conclusions

The specific method used to calibrate a particular model will vary depending on the model. For a given model, the appropriate calibration may also depend on location, due to varying performance of the model in different wave climates. It is emphasised again that the results presented here should not be interpreted as general results on the performance of WAM and WaveWatch III. Rather they are intended to illustrate how wave model errors should be treated when calculating wave energy statistics. However, it can be concluded that it is preferable to use offshore data from a hindcast rather than an archive of operational model runs, since this rules out changes in model performance due to changes in the operational model.

In the two datasets examined here, both had significant biases before calibration. After calibration, the WW3 hindcast seems to perform better, with no evidence of varying seasonal performance. The differences in estimate of monthly mean power between the calibrated WW3 hindcast and the buoy fall within the bounds predicted using the ARMA model of the error.

The use of an ARMA model proved not to be appropriate for estimating the errors in the calibrated WAM hindcast. This is most likely because the effects of changing seasonal performance were not accounted for initially. There was also evidence of interannual changes in the calibration of the WAM hindcast in summer during the calibration period.

Since there are only two years of buoy data concurrent with the models it is not possible to be sure what the causes are for the discrepancies between the models outside the calibration period.

One possibility is that changes to the operational WAM model at ECMWF may be responsible for some changes in the performance of the WAM/SWAN hindcast. Despite the fact the nearshore model used in the WW3 hindcast is driven by hindcast data, rather than operational data, we do not know whether the wind fields used to drive the WW3 hindcast are of consistent quality throughout. So we cannot rule out changes in the performance of the WW3 hindcast outside the calibration period.

Another reason for the observed differences between the hindcasts is that wave model performance is dependent on the wave conditions over the entire model domain, so changes in the seasonal or annual distributions of these conditions can cause changes in model biases. The error in a wave model estimate at a particular time is the cumulative result of errors which have occurred over the model grid and propagated to that location. It was shown that model biases vary depending on  $H_s$  and  $T_e$  (and doubtless on other variables not considered in this study), therefore changes in the distributions of these parameters over the entire domain will cause varying amounts of error to occur and propagate to the location in question. The large changes in wave conditions with seasons therefore results in seasonal changes in the model calibration. It would also seem likely that interannual changes in wave conditions cause interannual changes in model calibration. However, these should not be confused with the pseudo-effects described in Section 4.2.

The seasonal and interannual changes in the calibrations of the models make it difficult to quantify the uncertainty in the estimate of WEC yield. Although the ARMA representation of the errors in the WW3 hindcast appears valid for the calibration period, we cannot be certain that it gives a valid estimate of the uncertainty over the entire hindcast. A validation over a longer period, 10 years say, would be necessary before conclusions can be made about the long-term accuracy. From the results established in this paper it can be concluded that the uncertainty in the historic resource over a period of 8 years at this location is of the order of about 10 kW.

How does this compare to the accuracy which would be achievable from a continuous record of in-situ measurements? Suppose there is a long record of accurate in-situ measurements, from a buoy say, for a potential site of a wave farm. If a WEC had been placed close to the buoy, but not in the exact location, sampling variability will cause the power generated by the WEC to differ from that estimated from the buoy, even if we knew the exact response of a WEC to that sea state. By comparing estimates of power from two buoys at the EMEC site moored 1.5 km apart, Mackay [36] showed that the standard deviation of the differences in monthly mean power between the two buoys varied between about 0.5 kW and 2.5 kW, depending on the monthly mean power and the variability in wave conditions within the month. Comparing this to Fig. 18, it can be seen that the magnitude of the uncertainty caused by sampling variability is much smaller than that from errors in the model data.

It should also be noted that the accuracy which is currently achievable from model data is better than that which is theoretically achievable from satellite altimeter data alone (unless the number of altimeters in orbit increases in the future). Mackay et al. [37] showed that altimeter data can be used to estimate the power produced by a WEC and produce strategic-level maps of the long-term mean power produced. The main limiting factor to the accuracy of these maps was the limited temporal sampling from the altimeters. Mackay [36] investigated the accuracy that would theoretically be achievable if measurements from the altimeter missions to date were combined and used as the boundary conditions for a nearshore model. Due to the irregular nature of sampling from combined missions, it is not possible to give general results on the effect of limited temporal sampling. But using four case studies

it was shown that even if each boundary condition from the altimeter measurements gives a perfectly accurate estimate of WEC power at the target location, the limited temporal sampling would mean that the uncertainty in the monthly mean power is over double that from the calibrated model data.

Calibrating wave model data is a pragmatic solution to wave resource assessment using the data that is currently available. The calibrations are difficult to justify from a physical point of view. However there is a high level of empiricism already present in the model setup, so a further empirical calibration is not completely unreasonable. Improving the performance of the input wave models would be preferable to calibrating the outputs, but this is a much larger task. Both the WAM and WW3 models include assimilated altimeter measurements already, so it is difficult to see how any significant improvements could be made quickly. Nevertheless, the wave modelling community continually improves the performance of their models (see e.g. [19]) so some improvements can be expected in the future.

In the second article on uncertainty in wave energy resource assessment [6] we discuss how the interannual and climatic variability in wave conditions affects the predictability of WEC yield and how this compares to the uncertainty in the historic data. It is shown that uncertainty resulting from variability in the resource is of a similar magnitude to uncertainty in the historic data. This means that improving the accuracy of the historic data will result in improvements in the accuracy of predicted energy yield.

## Acknowledgements

The work presented here was partly funded under a Knowledge Transfer Partnership between Pelamis Wave Power Ltd, the University of Southampton and the National Oceanography Centre. The authors would like to thank Pelamis Wave Power Ltd for providing the hindcast data.

## References

- [1] Tucker MJ, Pitt EG. Waves in ocean engineering. London: Elsevier Science Ltd.; 2001.
- [2] Kerbiriou MA, Prevosto M, Maisondieu C, Clement A, Babarit A. Influence of sea-states description on wave energy production assessment. In: Proc. 7th European wave and tidal energy conference, Porto, Portugal; 2007.
- [3] Falcão AF. Wave-power absorption by a periodic linear array of oscillating water columns. *Ocean Engineering* 2002;29:1163–86.
- [4] Millar DL, Smith HCM, Reeve DE. Modelling analysis of the sensitivity of shoreline change to a wave farm. *Ocean Engineering* 2007;34:884–901.
- [5] Booij N, Ris RC, Holthuijsen LH. A third-generation wave model for coastal regions. 1: model description and validation. *Journal of Geophysical Research* 1999;104(C4):7649 (98JC02622).
- [6] Mackay EBL, Bahaj AS, Challenor PG. Uncertainty in wave energy resource assessment. Part 2: variability and predictability. *Renewable Energy* 2009;35(8):1809–19.
- [7] Defne Z, Haas KA, Fritz HM. Wave power potential along the Atlantic coast of the southeastern USA. *Renewable Energy* 2009;34:2197–205.
- [8] Dunnett D, Wallace JS. Electricity generation from wave power in Canada. *Renewable Energy* 2009;34:179–95.
- [9] Halliday JR, Douglas NG. Baseline survey of available wave data. The Crown Est. e, ISBN 978-1-906410-02-5; 2008. 126 pp.
- [10] Mollison D. Assessing the wave energy resource. pp.205–220 in, Statistics for the environment, 2: water related issues. In: Barnett V, Turkman KF, editors. Proc. SPRUCE II, Rothamsted experimental station, Harpenden, UK, 13–16 Sept 1993. Chichester: John Wiley & Sons; 1994. 391 pp.
- [11] Barstow S, Haug O, Krogstad HE. Satellite altimeter data in wave energy studies. *Ocean wave measurement and analysis*. In: Proc.3rd int. symp.: waves 97, 3–7 Nov 1997, vol. 1, Virginia Beach, USA; 1998, p. 339–54.
- [12] Pitt EG. The wave power climate at the wave hub site. *Applied Wave Research* 2006.
- [13] Iglesias G, Lopez M, Carballo R, Castro A, Fraguera JA, Frigaard P. Wave energy potential in Galicia (NW Spain). *Renewable Energy* 2009;34:2323–33.
- [14] Rusu E, Guedes Soares C. Numerical modelling to estimate the spatial distribution of the wave energy in the Portuguese nearshore. *Renewable Energy* 2009;34:1501–16.
- [15] Waters R, Engstrom J, Isberg J, Leijon M. Wave climate off the Swedish west coast. *Renewable Energy* 2009;34:1600–6.
- [16] Komen GJ, Cavaleri L, Donelan M, Hasselmann K, Hasselman S, Janssen PAEM. Dynamics and modelling of ocean waves. Cambridge University Press; 1994.
- [17] Cavaleri L, 25 co-authors. Wave modelling – the state of the art. *Progress in Oceanography* 2007;75:603–74.
- [18] Tolman HL. Validation of WAVEWATCH III version 1.15 for a global domain. Tech. rep. 213, NOAA natl. cent. for environ. predict. Camp Springs, MD; 2002.
- [19] Janssen PAEM. Progress in ocean wave forecasting. *Journal of Computational Physics* 2008;227:3572–94.
- [20] Bidlot JR, Holmes DJ, Wittmann PA, Lalbeharry R, Chen HS. Intercomparison of the performance of operational ocean wave forecasting systems with buoy data. *Weather and Forecasting* 2002;17:287–310.
- [21] Tolman HL, Balasubramanian B, Burroughs LD, Chalikov DV, Chao YY, Chen HS, et al. Development and implementation of wind generated ocean surface wave models at NCEP. *Weather and Forecasting* 2002;17:311–33.
- [22] Rogers WE, Wittmann PA, Wang DWC, Clancy RMC, Hsu YL. Evaluations of global wave prediction at the fleet numerical meteorology and oceanography center. *Weather and Forecasting* 2005;20(5):745–60.
- [23] Caires S, Sterl A. A new nonparametric method to correct model data: application to significant wave height from the ERA-40 re-analysis. *Journal of Atmospheric and Oceanic Technology* 2005;22(4):443–59.
- [24] Caires S, Sterl A. Validation of ocean wind and wave data using triple collocation. *Journal of Geophysical Research* 2003;108(C3):3098.
- [25] Janssen PAEM, Abdalla S, Hersbach H, Bidlot JR. Error estimation of buoy, satellite and model wave height data. *Journal of Atmospheric and Oceanic Technology* 2007;24:1665–77.
- [26] Swail VR, Cox AT. On the use of NCEP–NCAR reanalysis surface marine wind fields for a long-term North Atlantic wave hindcast. *Journal of Atmospheric and Oceanic Technology* 2000;17(4):532–45.
- [27] Swail VR, Ceccacci EA, Cox AT. The AES40 North Atlantic wave reanalysis: validation and climate assessment. In: Proc. 6th int. workshop on wave hindcasting and forecasting, November 6–10, Monterey, CA; 2000.
- [28] Cox AT, Swail VR. A 40-year global reanalysis of ocean waves 1958–1997 (GROW). *Journal of Geophysical Research* 2001;106(C2):2313–29.
- [29] Swail VR, Cardone VJ, Ferguson M, Gummer DJ, Harris EL, Orelup EA, et al. The MSC50 wind and wave reanalysis. In: Proc. 9th int. workshop on wave hindcasting and forecasting, September 25–29, 2006, Victoria, BC; 2006.
- [30] Tolman HL. Effect of observation errors in linear regression and bin-average analyses. *Quarterly Journal of the Royal Meteorological Society* 1998;124:897–917.
- [31] Donelan MA, Pierson WJ. The sampling variability of estimates of spectra of wind-generated waves. *Journal of Geophysical Research* 1983;88:4381–92.
- [32] Carter DJT, Tucker MJ. Uncertainties in environmental design criteria. *Underwater Technology* 1986;12:2–8. &33.
- [33] Young IR. Probability distribution of spectral integrals. *Journal of Waterway, Port, Coastal and Ocean Engineering* 1986;112(4):338–41.
- [34] Krogstad HE, Wolf J, Thompson SP, Wyatt LR. Methods for intercomparison of wave data. *Coastal Engineering* 1999;37:235–57.
- [35] Priestly MB. Spectral analysis and time series. London: Elsevier Academic Press; 1981.
- [36] Mackay EBL. Wave energy resource assessment. PhD thesis, University of Southampton; 2009.
- [37] Mackay EBL, Retzler CH, Challenor PG, Bahaj AS. Wave energy resource assessment using satellite altimeter data. In: Proc. ASME 27th int. conf. offshore mech. arctic eng. Paper number OMAE2008-57976; 2008.